energies

MDPI

Article

Design and Analysis of a Triple-Input Three-Level PV Inverter with Minimized Number of MPPT Controllers

Bikash Gyawali *, Rukhsar, Aidha Muhammad Ajmal and Yongheng Yang *

College of Electrical Engineering, Zhejiang University, Hangzhou 310027, China; rukhsar@zju.edu.cn (R.); ama@zju.edu.cn (A.M.A.)

* Correspondence: bikash_gyawali@zju.edu.cn (B.G.); yoy@zju.edu.cn (Y.Y.)

Abstract: Photovoltaic (PV) energy has been a preferable choice with the rise in global energy demand, as it is a sustainable, efficient, and cost-effective source of energy. Optimizing the power generation is necessary to fully utilize the PV system. Harvesting more power uses cascading of impedance source converters taking input from low-voltage PV arrays which requires multiple maximum power point tracking (MPPT) controllers. To solve this problem, a three-level inverter topology with a proposed PV arrangement, offering higher voltage boosting and a smaller size with a lower cost suitable for low-voltage panels, is designed in this article. The design criteria for parameters are discussed with the help of the small signal analysis. In this paper, three PV arrays are used to harvest maximum energy, which require only one MPPT controller and employ an extended perturb and observe (P&O) algorithm, being faster, highly efficient, and reducing the computational burden of the controller. Moreover, a three maximum power points tracker algorithm, which perturbs one parameter and observes six variables, is designed for the selected converter topology. Finally, the designed 1.1 kVA grid-connected PV system was simulated in MATLAB (R2023a) which shows that the MPPT algorithm offers better dynamics and is highly efficient with a conversion efficiency of 99.2% during uniform irradiance and 97% efficiency during variable irradiance conditions.

Keywords: maximum power point tracking; photovoltaic (PV) power systems; triple-input; three-phase; three-level; quasi-Z-source

check for updates

Citation: Gyawali, B.; Rukhsar; Ajmal, A.M.; Yang, Y. Design and Analysis of a Triple-Input Three-Level PV Inverter with Minimized Number of MPPT Controllers. *Energies* **2024**, *17*, 5380. https://doi.org/10.3390/en17215380

Academic Editors: José Matas and Ahmed Abu-Siada

Received: 8 October 2024
Revised: 20 October 2024
Accepted: 28 October 2024
Published: 29 October 2024

Copyright: © 2024 by the authors. Licensee MDPI, Basel, Switzerland. This article is an open access article distributed under the terms and conditions of the Creative Commons Attribution (CC BY) license (https://creativecommons.org/licenses/by/4.0/).

1. Introduction

Photovoltaic (PV) energy is one of the most promising ways to meet the increasing global energy demand. For the wide application of PV energy, the voltage generated from a low-voltage PV panel must be boosted and supplied to the grid. Several works have attempted to implement double-stage power conversion [1]. The voltage can be boosted separately to a required value; thus, the inverter design and controller become much easier. However, it has a challenge, especially under high duty cycle operation conditions, which reduces system efficiency [2,3]. In addition to that, it has several drawbacks like higher complexity, higher cost, reliability issues, impact on the dynamic response of the system, bigger size, and heavier weight which led to the invention and subsequent advancement of single-stage voltage boosting using quasi-Z-source inverters (qZSI) [4–6]. Using qZSI helps to reduce the circuit components which makes it highly compact. Voltage boosting and power inversion are possible in the qZSI due to the shoot-through (ST) in which all the switches in the same inverter leg can be short-circuited [7]. However, it is not possible in double-stage power converters. The qZSI topology can be used for PV applications that do not require an input capacitor due to the continuous input current generated from the PV panels. There has been advancement in the topology of the qZSI and an advantageous one is to use three-level topology, because it enables the harvest of more energy with higher efficiency [8].

Although much progress has been made with the implementation of three-level topology in PV systems [9], there are still some limitations in terms of common mode

voltage imbalance and leakage current flow [10]. Meanwhile, achieving the maximum power point (MPP) remains the most important issue using an appropriate algorithm [11]. There are several novel maximum power point tracking (MPPT) algorithms proposed to track the MPP for PV systems. These algorithms perform well, especially under partial shading conditions (PSCs) caused by shading of trees, buildings, dust, passing clouds, snow, and bird droppings [12,13]. Partial shading (PS) affects the performance and characteristics of PV panels by producing multi-peaks of MPP in the power–voltage (P–V) and current–voltage (I–V) curves. Traditional MPPT algorithms such as perturb and observe (P&O), hill climbing, and incremental conductance cannot operate at global maximum power point (GMPP) as they drift around the first maxima which may not be the GMPP. To overcome this issue, several optimization techniques such as the genetic algorithm, particle swarm optimization, ant colony optimization, artificial bee colony, and gray wolf optimization have been proposed [14]. These techniques can track the optimal MPP of the PV array when shading occurs. However, the efficiency is degraded as the operating point of the PV system moves away from the local maxima to obtain global maxima. To address this issue and to optimize efficiency and achieve better performance, the P&O algorithm can be modified and the number of MPPT controllers can be reduced. Reducing the number of MPPT controllers provides additional advantages like reduced cost and complexity.

Moreover, higher boosting is needed for grid-connected low-voltage PV modules to match the required AC voltage in the grid [15]. The three-level neutral-point-clamped quasi-Z-source inverter (3L-NPC-qZSI) is mostly preferred because it offers improved power quality which can be supplied to the grid [16]. In addition, the number of components used in the inverter topology is also reduced [17]. Also, the 3L-NPC-qZSI merges the strengths of a two-level topology, like reduced conduction losses and simplicity, with the benefits of a three-level topology. This makes it a viable option for specific low-voltage applications and also to connect with the grid because of its higher boosting ability [18].

In this paper, a triple-input three-level neutral-point-clamped quasi-Z-source inverter (TI-3L-NPC-qZSI) is developed as shown in Figure 1. The three-level inverter topology is selected because of its ability to supply power with high quality. The paper's main focus is to design a highly efficient and robust rooftop PV system while harvesting the maximum possible energy from multiple PV panels that generate low voltage. In addition, energy can be harvested with multiple PV inputs utilizimg only one MPPT controller, resulting in a more cost-effective solution.

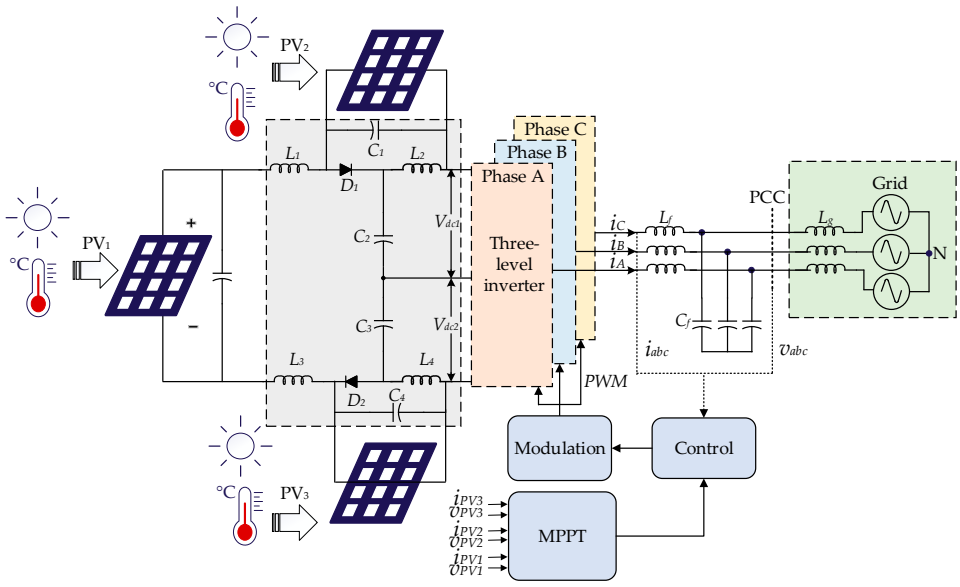

Figure 1. Triple-input three-level neutral-point-clamped quasi-Z-source inverter connected to grid.

The rest of this paper is organized as follows: Section 2 presents the proposed PV arrangement for the TI-3L-NPC-qZSI topology and its operational conditions. Section 3 performs dynamic modeling and small signal analysis to ensure that the proposed system is stable, reliable, and operates efficiently. Section 4 presents the topology's parameter design. Section 5 illustrates the implemented MPPT algorithm. Section 6 presents the simulation results and discussion. Section 7 compares the implemented topology with other similar topologies proposed in the literature. Section 8 concludes the paper.

2. System Description

The proposed novel arrangement is presented in Figure 1, in which two additional PV arrays, PV_2 and PV_3, have been added to the upper and lower quasi-Z-source (qZS) network. The upper qZS network has two inductors, two capacitors, and a diode. Similarly, the lower qZSI is a replica of the upper qZS network. The current and voltage of all three PV panels are sensed for the MPPT controller and the grid voltage and current are sensed for the AC controller. Finally, the generated pulse width modulation (PWM) signal is fed to the inverter switches. The state of these switches decides the operation mode of the inverter. The detailed circuit for the TI-3L-NPC-qZSI topology is shown in Figure 2.

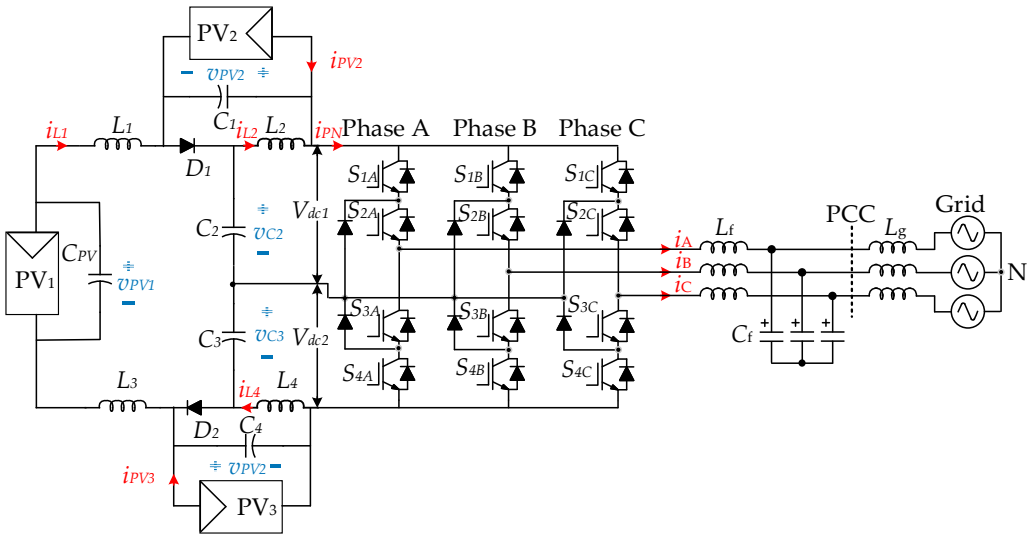

Figure 2. Equivalent circuit for the TI-3L-NPC-qZSI.

To investigate the TI-3L-NPC-qZSI, the equivalent circuits of the converter during full-ST (FST), non-ST (NST), upper-ST (UST), and lower-ST (LST) are presented in Figure 3. During the FST, as illustrated in Figure 3a, one of the converter legs is short-circuited, increasing the current in the impedance network as the capacitor discharges, moving the PV array's operating points closer to their short-circuit currents. According to Figure 3a, the energy stored in the CPV is released to L_1, whereas the energy of C_2 and C_3 are discharged into L_2 and L_3, respectively. Similarly, as shown in Figure 3c,d, for the UST and LST, the upper and lower two switches will be short-circuited, respectively. The capacitor voltage is discharged in both of the ST states. After the ST, when the active state starts, the capacitors charge again until the inductor current is finished. As shown in Figure 3b, PV_1, L_1, and L_3, boost C_2 voltage and C_3 voltage, and PV_2 and L_2 boost C_1 voltage. Similarly, PV_3 and L_4 boost C_4 voltage. The generated power is simultaneously supplied to the grid through the TI-3L-NPC-qZSI.

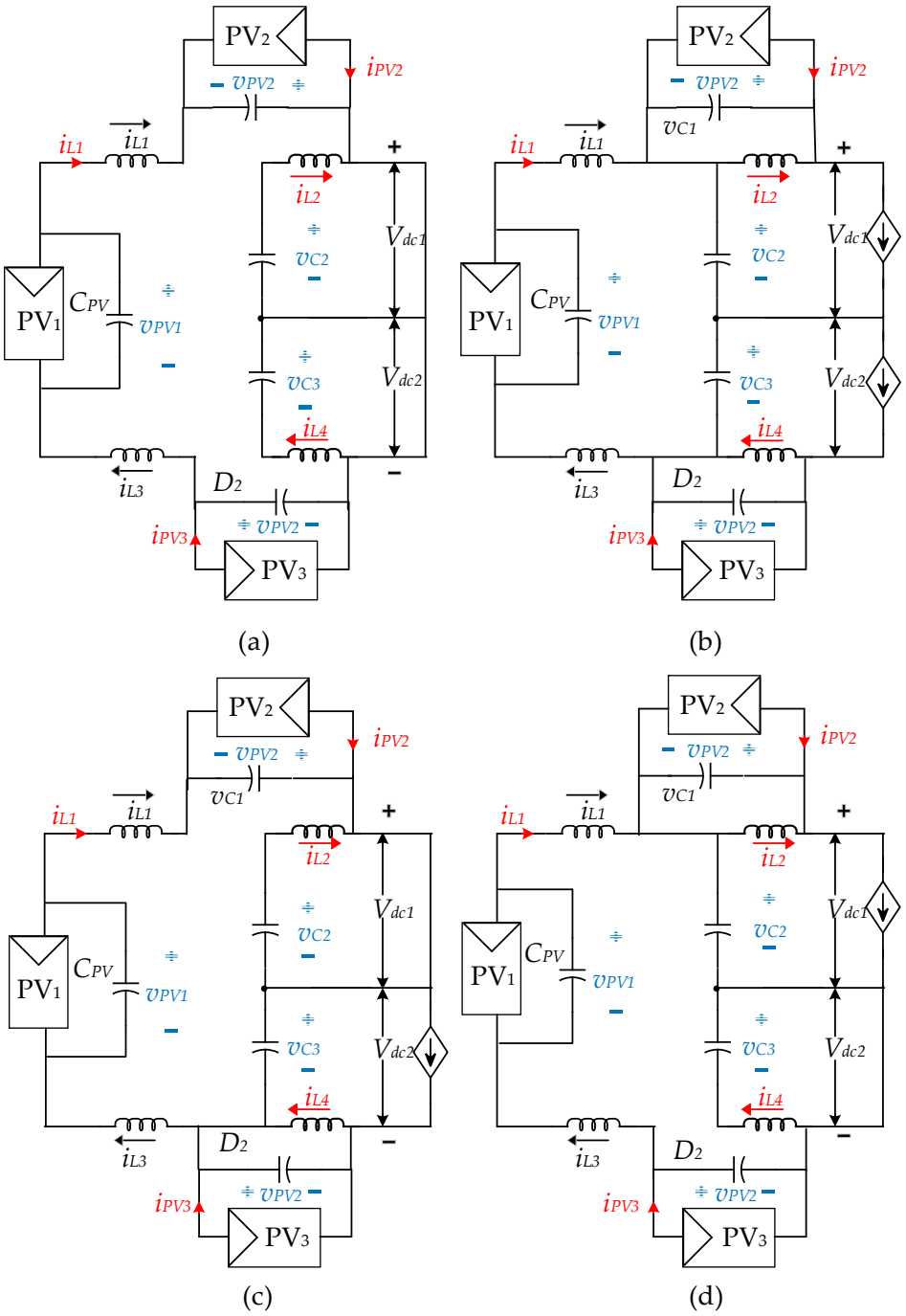

Figure 3. Operational modes (equivalent circuits) of the TI-3L-NPC-qZSI topology. (**a**) FST, (**b**) NST, (**c**) UST, and (**d**) LST.

3. Dynamic Modeling

The small signal analysis and modeling are carried out with the following assumptions:

- The inductances and capacitances of the qZSI are equal and indicated as L and C, respectively;
- Continuous conduction;
- Lossy capacitor and inductors with resistance R_C and R_L, respectively;
- Diodes and switches are ideal.

During the ST state (t_{st}), energy stored in capacitors is transferred to inductors, and during the NST state (t_{nst}), sources (i.e., PV panels) charge the capacitors and supply the load, as input diodes conduct. Inductors are discharged through loads and thereby boost

the DC-link voltage. The total switching time (t_s) is the sum of ST and NST states, i.e., $t_s = t_{st} + t_{nst}$. State vector (x) is formed using the currents of inductor L_1 (i_{L1}) and L_2 (i_{L2}) and the voltages of the capacitor C_2 (v_{C2}) and PV_2 (v_{PV2}). Similarly, the input vector (u) is formed using the voltage of PV_1 (v_{PV1}), the current of PV_2 (i_{PV2}), and the DC-link current (i_{PN}).

The state vector is

$$x = [i_{L1}\ i_{L2}\ v_{C2}\ v_{PV2}]^T \tag{1}$$

and the input vector is

$$u = [v_{PV1}\ i_{PV2}\ i_{PN}]^T \tag{2}$$

Subsequently, the state-space equations in ST and NST modes are obtained as

$$\dot{x} = A_0 x + B_0 u \tag{3}$$

$$\dot{x} = A_1 x + B_1 u \tag{4}$$

where

$$A_0 = \begin{bmatrix} -(R_L + R_C/L) & 0 & 0 & 1/L \\ 0 & -(R_L + R_C/L) & 1/L & 0 \\ 0 & -1/C & 0 & 0 \\ -1/C & 0 & 0 & 0 \end{bmatrix},$$

$$B_0 = \begin{bmatrix} 1/2L & 0 & 0 \\ 0 & 0 & 0 \\ 0 & 0 & 0 \\ 0 & \frac{1}{2L} & 0 \end{bmatrix},$$

$$A_1 = \begin{bmatrix} -(R_L + R_C/L) & 0 & -1/L & 0 \\ 0 & -(R_L + R_C/L) & 0 & -1/L \\ 1/C & 0 & 0 & 0 \\ 0 & 1/C & 0 & 0 \end{bmatrix},$$

and

$$B_1 = \begin{bmatrix} 1/2L & 0 & RC/L \\ 0 & 0 & RC/L \\ 0 & 0 & -1/C \\ 0 & 1/2L & -1/C \end{bmatrix}$$

Using (3) and (4) over a complete switching cycle of t_s for average, the average state-space model can be obtained as

$$\dot{x} = Ax + Bu \tag{5}$$

$$y = Cx + Eu \tag{6}$$

in which $A = d_{st}A_0 + d_{nst}A_1$, $B = d_{st}B_0 + d_{nst}B_1$, d_{st} is the ST duty ratio, and d_{nst} is the NST duty ratio with

$$A = \begin{bmatrix} -(R_L + R_C/L) & 0 & d_{st} - 1/L & d_{st}/L \\ 0 & -(R_L + R_C/L) & d_{st}/L & d_{st} - 1/L \\ 1 - d_{st}/C & -d_{st}/C & 0 & 0 \\ -d_{st}/C & 1 - D_{st}/C & 0 & 0 \end{bmatrix},$$

and

$$B = \begin{bmatrix} 1/2L & 0 & RC(1-d_{st})/L \\ 0 & 0 & RC(1-d_{st})/L \\ 0 & 0 & d_{st} - 1/L \\ 0 & 1/2L & d_{st} - 1/L \end{bmatrix}$$

The small signal model of the proposed TI-3L-NPC-qZSI can be obtained by applying the Laplace transform on (3) and (4), with the introduction of perturbation on v_{PV_1}, i_{PV_2}, and i_{PN}. Each of these signals is substituted with the addition of the equilibrium point and induced perturbation, i.e., $u = U + \tilde{u}$, which finally induces $x = U + \tilde{x}$. The transfer function from $\tilde{d}_{\mathrm{st}}$ to $\tilde{i}_{\mathrm{L1}}$ is used in investigating the system stability and parameter design. The assumption made for the analytical calculation of the transfer function includes $i_{L1} = i_{L3}$, $i_{L2} = i_{L4}$, $v_{C2} = v_{C3}$, $v_{PV2} = v_{PV3}$, $v_{dc1} = v_{dc2}$.

$$G_{\tilde{d}_{\mathrm{st}}}^{\tilde{i}_{\mathrm{L1}}}(s) = \left.\frac{\tilde{i}_{\mathrm{L1}}}{\tilde{d}_{\mathrm{sh}}}\right|_{\substack{\tilde{i}_{\mathrm{PN}}=0 \\ \tilde{i}_{\mathrm{PV2}}=0 \\ \tilde{i}_{\mathrm{PV1}}=0}} = \frac{(n_1 s + n_2)}{LCs^2 + C(R_L + R_C)s + (d_{\mathrm{nst}} - d_{\mathrm{st}})} \tag{7}$$

where $n_1 = (v_{C1} + v_{C2})\mathrm{C}$ and $n_2 = 4L(i_{\mathrm{PN}} - i_{\mathrm{L1}} - i_{\mathrm{L2}}) + (d_{\mathrm{nst}} - d_{\mathrm{st}})$. The transfer function from $\tilde{i}_{\mathrm{L1}}$ to $\tilde{v}_{\mathrm{PV1}}$, $G_{\tilde{i}_{\mathrm{L1}}}^{\tilde{v}_{\mathrm{PV1}}}(s)$ can be obtained by converting the formula obtained by Kirchhoff's law applied to the input of the TI-3L-NPC-qZSI into the Laplace domain

$$G_{\tilde{i}_{\mathrm{L1}}}^{\tilde{v}_{\mathrm{PV1}}}(s) = \left.\frac{\tilde{v}_{\mathrm{PV1}}}{\tilde{i}_{\mathrm{PV1}} - \tilde{i}_{\mathrm{L1}}}\right|_{\substack{\tilde{i}_{\mathrm{PN}}=0 \\ \tilde{i}_{\mathrm{PV2}}=0 \\ \tilde{i}_{\mathrm{PV1}}=0}} = \frac{1}{\mathrm{C_{PV}s}} \tag{8}$$

Accordingly, the block diagram of the closed-loop control of the TI-3L-NPC-qZSI model in the Laplace domain can be obtained as shown in Figure 4. The transfer function $G_{\tilde{d}_{st}}^{\tilde{i}_{L1}}(s)$ is derived similarly as it is for a basic qZSI topology [19]. However, the relationship of inductor current varies. Taking the relation from (5), the relation of all the inductor currents can be derived as $i_{PV2} = i_{L1} - i_{L2}$ and $i_{PV3} = i_{L4} - i_{L3}$.

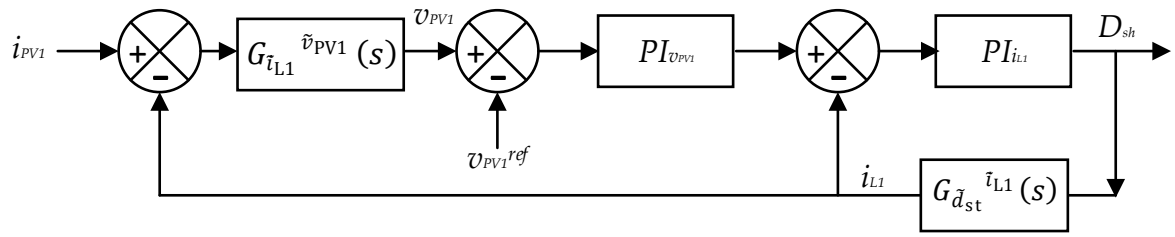

Figure 4. Block diagram of the closed-loop control of the PV system.

The Bode plots of the obtained transfer functions $G_{\tilde{d}_{\mathrm{st}}}^{\tilde{i}_{\mathrm{L1}}}(s)$ and $G_{\tilde{i}_{\mathrm{L1}}}^{\tilde{v}_{\mathrm{PV1}}}(s)$ with their product K(s) (being the transfer function from the duty cycle, i.e., $G_{\tilde{d}_{\mathrm{st}}}^{\tilde{i}_{\mathrm{L1}}}(s)$ to the PV voltage $\tilde{v}_{\mathrm{PV1}}$) are shown in Figure 5a, which shows the gain crossover frequency (ω_{gc}) being 1100 rad/s. And, Figure 5b suggests a ω_{gc} of 999 rad/s, phase margin of 80°, and gain margin of 37 dB to the corresponding closed-loop frequency response. In addition, the root loci of the transfer function $G_{\tilde{d}_{\mathrm{st}}}^{\tilde{i}_{\mathrm{L1}}}(s)$ is shown in Figure 6.

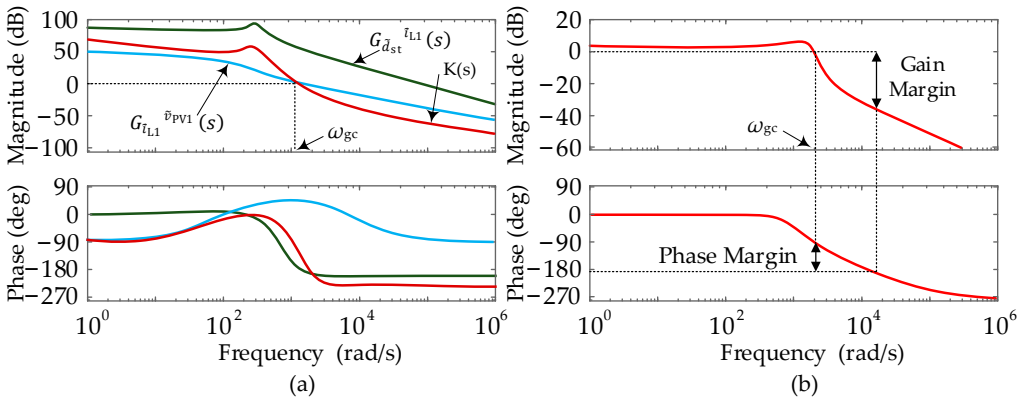

Figure 5. Frequency response of the control: (**a**) open-loop Bode plot of $G_{\tilde{d}_{st}}^{\tilde{i}_{L1}}(s)$, $G_{\tilde{i}_{L1}}^{\tilde{v}_{PV1}}(s)$ and K(s); (**b**) closed-loop Bode plot of the corresponding system.

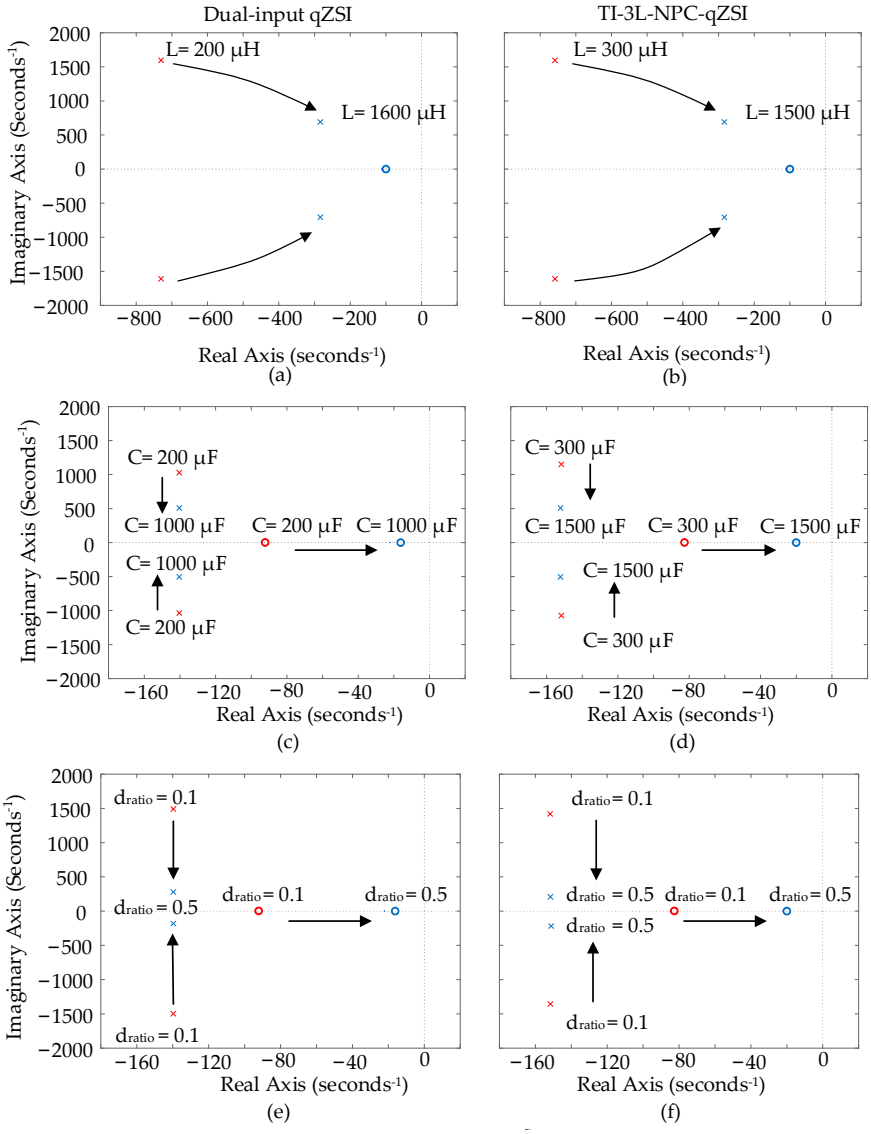

Figure 6. The root loci of the transfer function $G_{\tilde{d}_{st}}^{\tilde{i}_{L1}}(s)$. (**a**) Inductor (L), (**c**) capacitor (C), and (**e**) duty ratio (D) sweeps in the dual-input qZSI. (**b**) Inductor (L), (**d**) capacitor (C), and (**f**) duty ratio (d_{ratio}) sweeps in the TI-3L-NPC-qZSI (Circles indicate zeros and cross indicates poles, while increasing value of parameter is indicated by changing color from red to blue).

Values for the inductor, capacitor, and ST duty ratio are increased in the direction of the arrow and the dynamic characteristics are observed. The system is designed with the parameters being v_{PV1} = 73 V, i_{PV2} = 5 A, d_{st} = 0.25, $C_{1,2}$ = 1.5 mF, $L_{1,2}$ = 1.5 mH R_C = 0.42 Ω, and R_L = 0.1Ω. Using the Ziegler and Nichols method, the proportional (k_p) and integral (k_i) gains of $G_{\tilde{i}_{L1}}^{\tilde{v}_{PV1}}(s)$ are taken as 0.1 and 45, respectively, and for $G_{\tilde{d}_{sh}}^{\tilde{i}_{L1}}(s)$ are taken as 0.05 and 2, respectively [20]. When the root loci of the TI-3L-NPC-qZSI is compared with the root loci of the dual-input qZSI, the stability of both the systems is observed to be equally fine [21]. Poles and zeros are on the left half plane. The closed-loop system is stable and in addition to that its boosting ability is the best among its competing converter topologies. A comparison of the boost factor with those topologies is shown in Figure 7. Hence, this topology is promising among various converter topologies [9,15,19,22]. The design of this topology is performed in the next section.

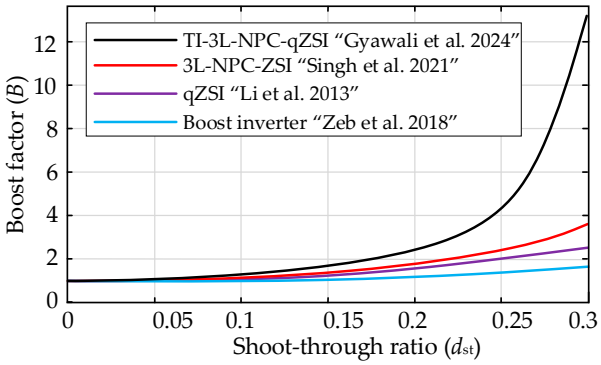

Figure 7. Comparison of the boosting capability of various inverter topologies [9,15,19,22].

4. Design of the TI-3L-NPC-qZSI Topology

Inductors are designed in such a way that they are able to limit the current during the ST process. Using (4), the desired relationship for inductors can be derived [5].

$$L_1 = L_2 = L_3 = L_4 = v_{C2}\frac{dt_{st}}{di_{L1}} = v_{C3}\frac{dt_{st}}{di_{L1}} = \frac{\Delta t_{st}}{\Delta i_{L1}}(v_{PV1} + v_{PV2} + v_{PV3}) \tag{9}$$

$$\Delta t_{st} = \frac{d_{st}}{nf_s} \tag{10}$$

where f_s is the switching frequency, n is the number of ST states that happen in one switching period, and Δt_{st} is the maximum ST duration.

Capacitors absorb the currents going through the diode (D) during the active state, which is, according to Figure 3b and Kirchhoff's current law, estimated as

$$i_{L1} - C_1\frac{dv_{PV2}}{dt} = C_2\frac{d(v_{PV1} + v_{PV2})}{dt} \tag{11}$$

$$i_{L3} - C_4\frac{dv_{PV3}}{dt} = C_3\frac{d(v_{PV1} + v_{PV2})}{dt} \tag{12}$$

The capacitance of all capacitors (C_1, C_2, C_2, *and* C_4) must be equal in order to avoid resonance in the qZS network [23]. The feature of these capacitors includes the filtering of high frequency ripple caused by switches and low frequency caused by oscillatory instantaneous power. From (11) and (12), the capacitor values can be designed as

$$C_1 = C_2 = C_2 = C_4 = \frac{i_{L1}}{6f_g(\Delta v_{PV1} + \Delta v_{PV2} + \Delta v_{PV3})} \tag{13}$$

where $\Delta v_{PV1}, \Delta v_{PV2}, and\ \Delta v_{PV3}$ are the allowable ripple voltage for PV_1, PV_2, and PV_3, and f_g is the grid frequency.

Additionally, the PV parameter is of importance. Using (4) and equating it with zero for steady state condition gives

$$v_{PV2} = v_{PV3} = v_{PV1}\frac{d_{st}}{1 - d_{st}} \tag{14}$$

$$i_{PV1} = \frac{(d_{nst} - d_{st})i_{PN} - d_{st}i_{PV2}}{d_{nst} - d_{st}} \tag{15}$$

It is obvious in (14) and (15) that the duty ratio is greater than zero. Hence, $i_{PV1} \geq i_{PV2} \approx i_{PV3}$ and when $d_{st} = 0.25$, v_{PV1} is double of v_{PV2}. There are other things to be considered while designing the topology: (1) The power generation from PV_1 must be greater than the other two to ensure $i_{PV1} \geq i_{PV2}$. (2) The power generation from PV_2 and PV_3 should be equal to $i_{PV2} \approx i_{PV3}$. (3) The neutral point voltage, v_{PV2} and v_{PV3}, from PV_2 and PV_3 panels should be equal.

5. Extended MPPT Algorithm

Achieving maximum power is both a challenging and important task. The main objective is to reduce the complexity and cost by using only one controller to control three PV panels. In order to optimize the power generated from the PV panel, one must track the maximum power generated by the panel and achieve it using an efficient algorithm. Several MPPT algorithms have been reported [14,24,25] to solve the issues. The P&O algorithm is preferred because of its cost-effectiveness. Moreover, optimizing and tracking the maximum power generated by three panels connected to a single converter needs some modifications in the control algorithm. Therefore, an extended P&O algorithm is implemented to the proposed topology (see Figure 1), and the flowchart of the extended MPPT algorithm is presented in Figure 8. The sampling frequency of the MPPT controller is set to 20 Hz and the increment Δv is taken as 1 V for the perturbation. The perturbation on PV_1 has an effect on the other two panels. Both panels' observation processes are based on the perturbation of PV_1 and with themselves as well. Hence, the reference voltage from the PV_1 is taken to generate the reference voltage for the controller. Due to this, separate MPPT controllers are not appropriate for keeping the connection between all the panels. As such, a single MPPT controller with the ability to track the maximum power by considering the impact of perturbation on each other is implemented in the following. As shown in Figure 9, the MPP is achieved with the extended P&O algorithm shown in Figure 8 during standard test conditions (STCs) and PSCs with PV_1 at 600 W/m^2, PV_2 at 800 W/m^2, and PV_3 at 1000 W/m^2. The extended P&O works basically by perturbing the operating voltage and observing the power variation. This leads the operating point towards the MPP.

The MPP can be tracked when the following conditions are achieved:

$$\frac{dP_{PV}}{dv_{PV}} = 0 \text{ (At MPP)} \tag{16}$$

$$\frac{dP_{PV}}{dv_{PV}} > 0 \text{ (On the left side of MPP)} \tag{17}$$

$$\frac{dP_{PV}}{dv_{PV}} < 0 \text{ (On the right side of MPP)} \tag{18}$$

The fluctuations in voltage of both the panels PV_2 and PV_3 are used in the same sampling period for the self-perturbation of PV_2 and PV_3. The correct tracking direction is decided according to the change in the reference voltage in the positive or negative direction. Similarly, the perturbation with respect to PV_1 is performed in an alternative

sampling period. Here, the change of the reference voltage is governed by two closed-loop controls, as shown in Figure 10:

$$v_{ref} = v_{ref} \pm \Delta v \tag{19}$$

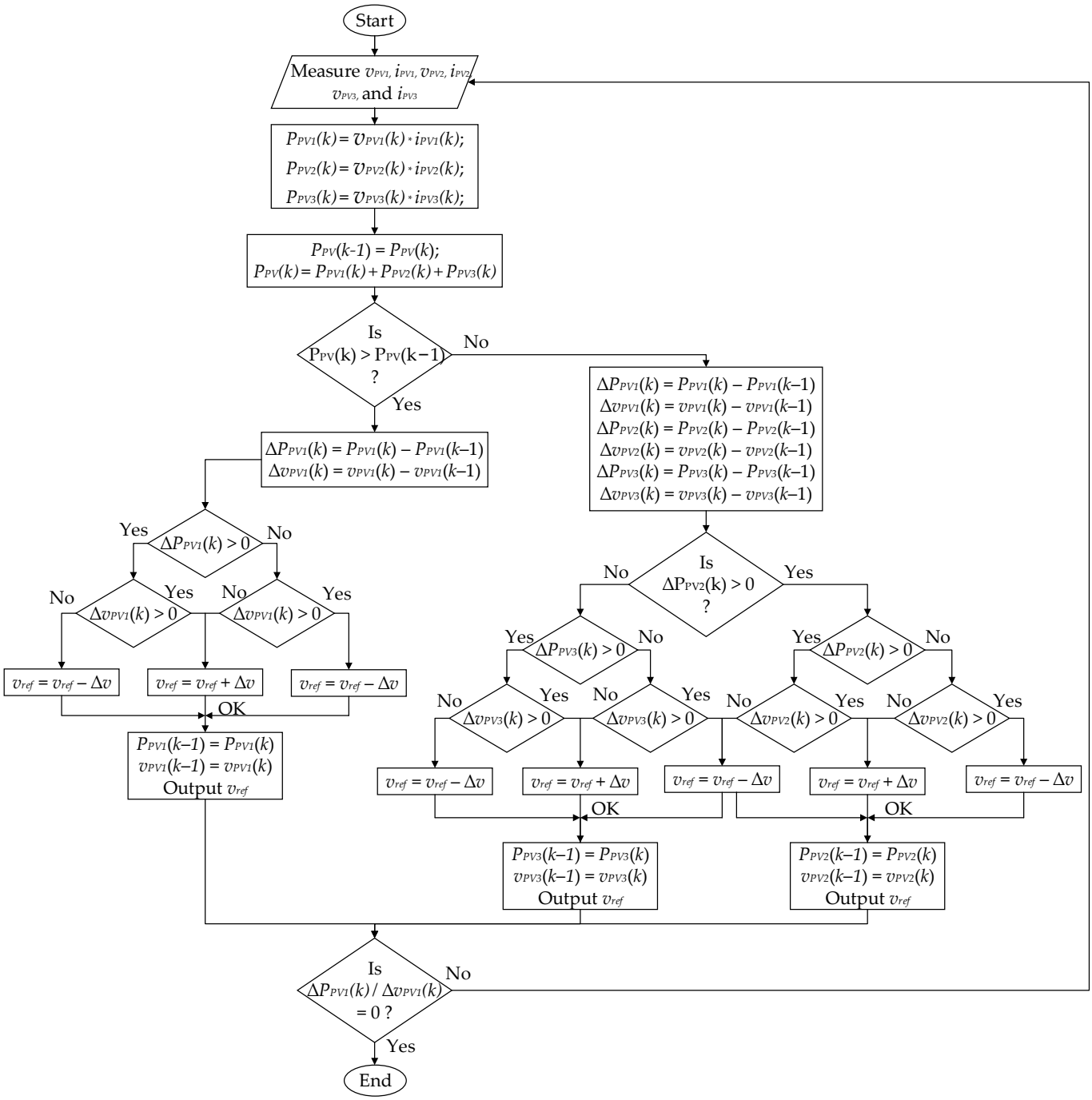

Figure 8. Extended perturb and observe algorithm for the TI-3L-NPC-qZSI system.

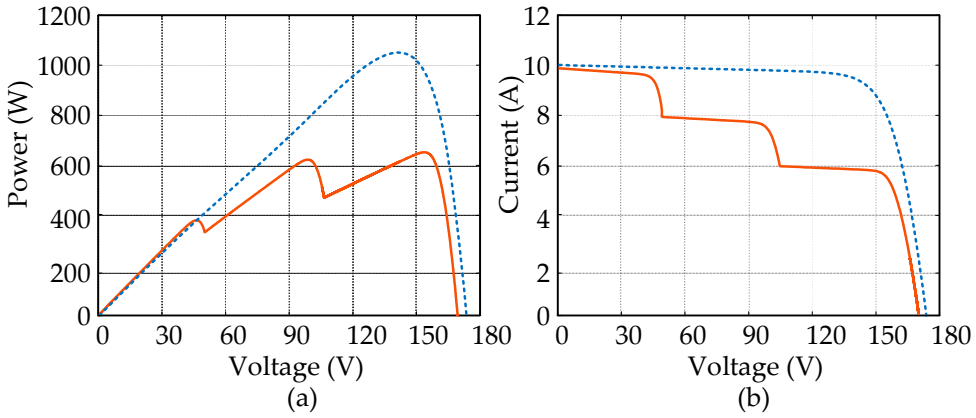

Figure 9. Plot during STCs (dash line) and during PSCs (solid line) (**a**) P–V curve, and (**b**) I–V curve.

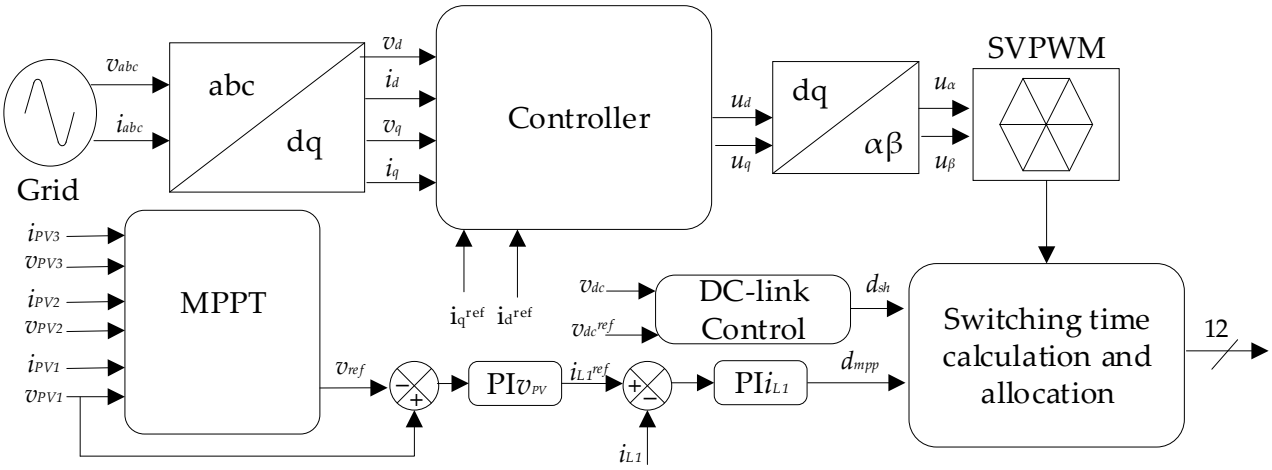

Figure 10. Control strategy of the TI-3L-NPC-qZSI connected to the grid [6,22].

However, both the self-perturbation and perturbation with respect to PV_1 are performed. The one with the higher impact on the reference voltage is selected to achieve the MPP faster. Finally, the MPPT controller generates a reference voltage which is used to obtain the ST ratio at the MPP which is utilized to calculate the switching time.

6. Simulation Results and Discussion

The PV system as depicted in Figure 1 is built in MATLAB and the simulation work is performed based on the parameters shown in Table 1. The panel PV_1 has two strings with two series modules and both PV_2 and PV_3 panels have a string with a single module. Initially, the simulation is performed at STC, and after that, different irradiance for PV_1, PV_2, and PV_3 is taken into consideration to explore its impact on the power generation. Simulation results are shown in Figures 11–13 for PV_1, PV_2, and PV_3, respectively.

It has been shown that the power generation from PV_1 must be greater than both of the other panels and the identical panel rating is used for PV_2 and PV_3 because the generated voltage from these panels must meet the criteria as discussed in Section 4. From the simulation results, it is observed that the change in irradiance on the first PV array affects power generation in all other PV arrays and the power generation of PV_3 is also affected by PV_2. The power ripple during the steady state is of 2 W. Also, the power value achieves the steady state quickly which shows that the controller provides fast dynamics. PS is encountered in PV_2 while there is no shading on PV_3, and to balance the neutral point voltage and to balance the capacitor voltage, the power generation of both panels is limited to the generation of PV_2. As obtained from the simulation results, the power achieved during the STCs and PSCs has been presented in Table 2.

Table 1. Parameter values used for the TI-3L-NPC-qZSI topology.

Inverter Topology		
Parameter	**Symbol**	**Values**
Inductor	L_1	1 mH
	L_2	1 mH
	L_3	1 mH
	L_4	1 mH
Capacitor	C_1	1.5 mF
	C_2	1.5 mF
	C_3	1.5 mF
	C_4	1.5 mF
Output Filter	$R_f + L_f$	0.1 Ω + 3.5 mH
	$R_f + C_f$	0.42 Ω + 7.505 µF
Switching frequency	f_s	10 kHz
Inverter Rating	S	1 kW
PV module parameter		
Number of PV cells	N_s	72
MPP voltage at STC	$V_{\text{mpp,stc}}$	36.72 V
MPP current at STC	$I_{\text{mpp,stc}}$	4.9 A
MPP power at STC	$P_{\text{mpp,stc}}$	179.928 W
Open-circuit voltage at STC	$V_{\text{oc,stc}}$	44.06 V
Short-circuit current at STC	$I_{\text{sc,stc}}$	5.31 A
Temperature coefficient of V_{OC}	$\beta_{V_{oc}}$	−0.3616 mV/°C
Temperature coefficient of I_{SC}	$\beta_{I_{sc}}$	0.041507%/°C

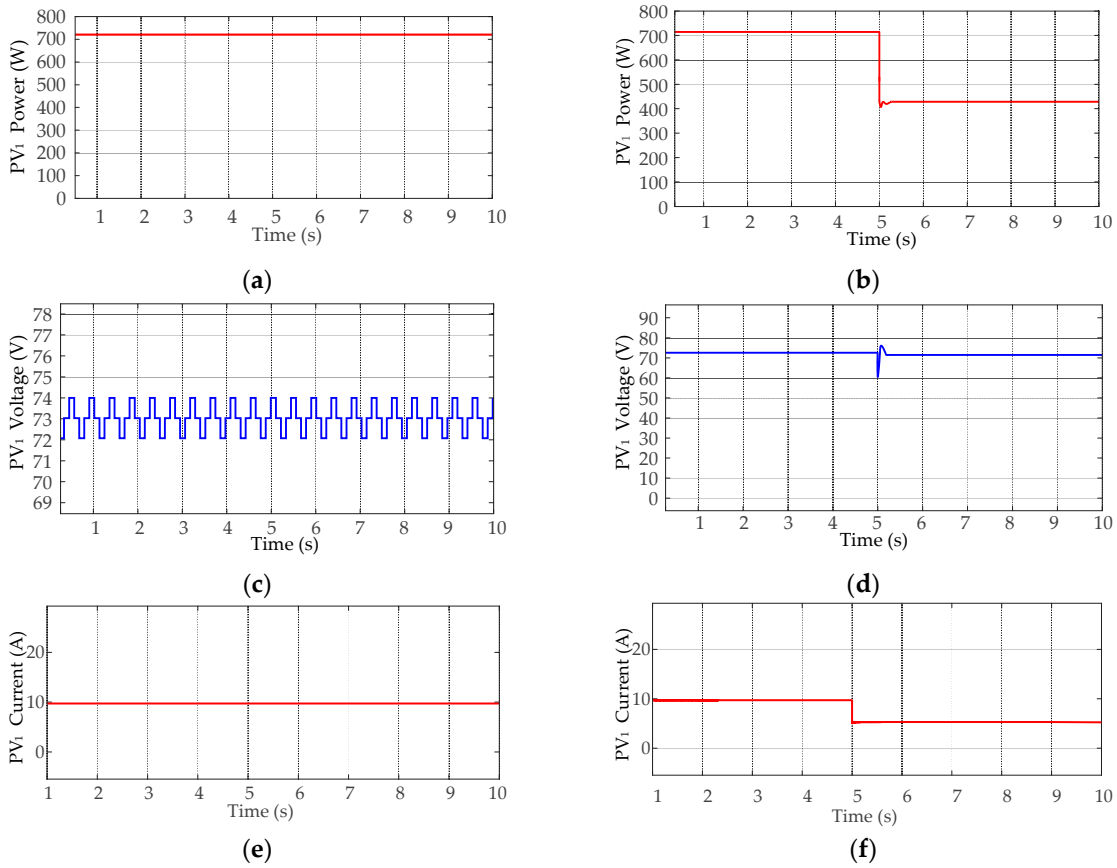

Figure 11. PV_1 at STCs: (**a**) power, (**c**) voltage, and (**e**) current. Dynamic test of PV_1 (**b**) power, (**d**) voltage, and (**f**) current.

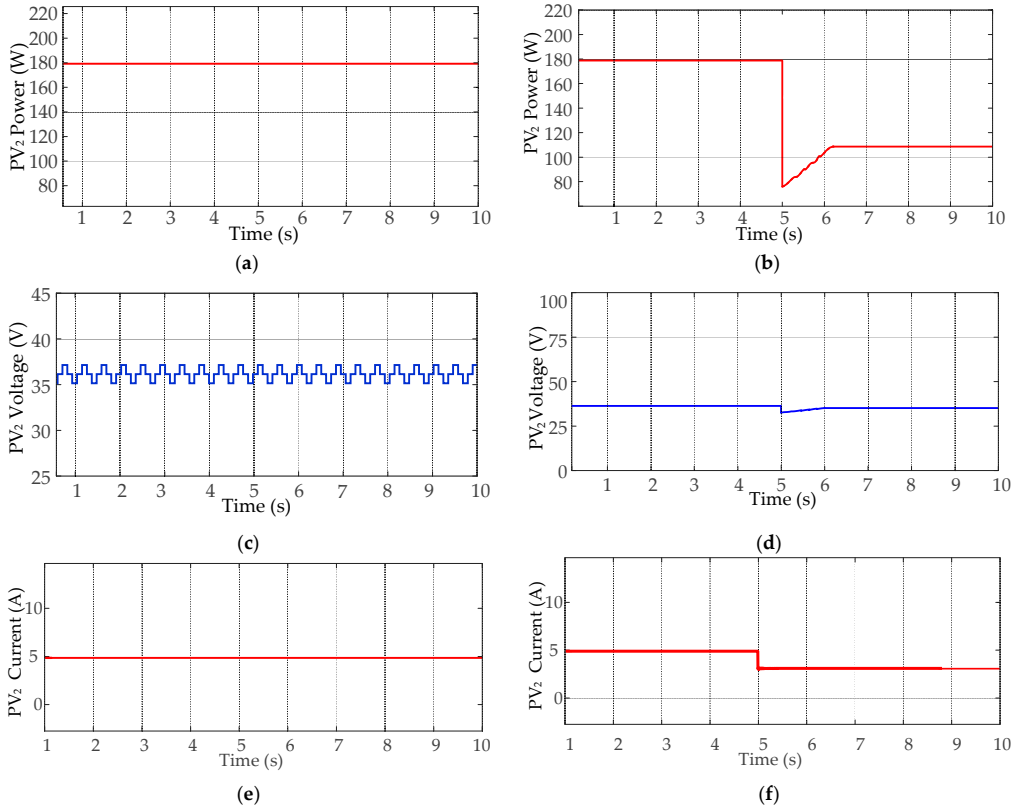

Figure 12. PV_2 at STCs: (**a**) power, (**c**) voltage, and (**e**) current. Dynamic test of PV_2 (**b**) power, (**d**) voltage, and (**f**) current.

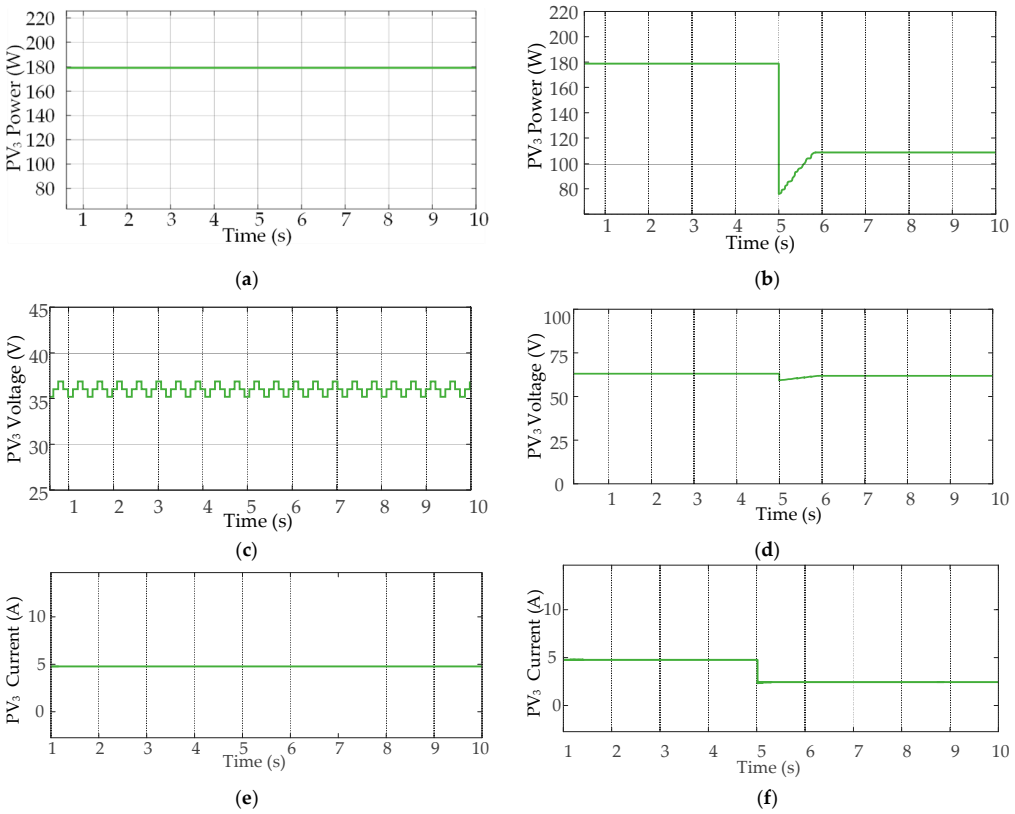

Figure 13. PV_3 at STCs: (**a**) power, (**c**) voltage, and (**e**) current. Dynamic test of PV_3 (**b**) power, (**d**) voltage, and (**f**) current.

Table 2. Power achieved during the partial shading condition.

PV Array	Achieved Power During STCs	Achieved Power During PSCs
PV_1	719 W	427 W
PV_2	179 W	107 W
PV_3	179 W	107 W

The theoretical value of the power for a single module during the STCs is tabulated in Table 1. Comparing the theoretical value of power with the achieved maximum power values, the efficiency can be calculated [26] as

$$\eta_{MPPT} = \frac{\int_0^t P_{PV}(t)dt}{\int_0^t P_{mpp}(t)dt} \times 100\% \quad (20)$$

where η_{MPPT} represents the MPPT efficiency, P_{mpp} represents theoretical maximum power, and P_{PV} represents the achieved maximum power. The highest MPPT efficiency of 99.2% is achieved during STCs and the maximum conversion efficiency of 97% is achieved during PSCs for the presented PV system with the extended P&O MPPT algorithm.

7. Comparative Analysis

In Table 3, the comparison of the implemented topology with the other topologies that are already proposed by various researchers is presented. The comparison is conducted in terms of the number of MPPT controllers used (N_{MPPT}), number of PV inputs used to harvest energy (N_{input}), number of phases (N_{P}), component count, inverter level, energy harvesting, controller cost, and switching frequency (f_{s}), as well as whether it uses a neutral-point-clamped (NPC) inverter or not (for better power quality). In [19], a voltage-fed two-level qZSI has been presented for PV systems connected to the grid. In [27], two PV inputs have been used to harvest maximum energy utilizing a unique three-level inverter topology which is the combination of two DC-DC buck-boost converters. In [28], a grid-connected 3L-NPC-qZSI is utilized to harvest energy from a single PV input. In [21], a grid-connected two-level qZSI is utilized to harvest energy from two PV inputs. While comparing all of these inverter topologies with the TI-3L-NPC-qZSI, it is clear that the number of MPPT controllers can be minimized for multiple PV inputs according to the system requirements without affecting the overall performance of the PV system.

Table 3. Comparison of the proposed topology with other famous topologies.

Factors	Reference [19]	Reference [27]	Reference [28]	Reference [21]	Implemented
N_{MPPT}	1	2	1	1	1
N_{input}	1	2	1	2	3
N_{P}	3	1	3	3	3
Active switches	6	6	12	6	12
Inverter level	2	2	3	2	3
Energy Harvesting	Low	Medium	Low	Medium	High
Controller cost	High	High	High	Medium	Low
f_{s}	Medium	High	High	High	High
NPC	No	Yes	Yes	No	Yes

To assess the overall enhancement in performance of a PV system when utilizing different MPPT algorithms, a qualitative comparison can be conducted based on factors such as steady-state power ripple, MPPT control response dynamics, fill-factor (FF), mismatch losses, system complexity, and MPPT efficiency, as shown in Table 4. Steady-state

power ripple is the fluctuation of power allowed in the steady state value of the maximum achieved power. Power ripple can be limited to a small value while designing the MPPT controller. Similarly, the dynamics of the system must be faster to quickly achieve the MPPT. In addition, the FF is the measure of efficient energy conversion and the PSCs in the PV cause the variation in the FF. The FF is another factor used to study the power losses during the influence of shading for PV systems. The FF is determined as

$$\%FF = \frac{P_{mpp}}{V_{oc} \times I_{sc}} \times 100 \quad (21)$$

where $\%FF$ is the percentage fill-factor, P_{mpp} is the maximum power, V_{oc} is the open-circuit voltage, and I_{sc} is the short-circuit current.

Table 4. Qualitative comparison of proposed topology with a dual-input qZSI.

Factors	Dual-Input qZSI [21]	GUANYA Inverter [20]	Implemented
Power ripple	3 W (0.0015% of P_{mpp})	6 W (0.0031% of P_{mpp})	2 W (0.0027% of P_{mpp})
Dynamics (Time required to reach steady state after encountering shading)	PV_1 = 0.35 s PV_2 = 3 s	PV = 0.38 s	PV1 = 0.2 s PV2 = 1.1 s PV3 = 0.9 s
$\%FF$	67%	75%	72%
$\%\Delta P_{loss}$	36%	39%	35%
Complexity	Medium	Low	Low
η_{MPPT}	96.21%	95%	97.097%

Similarly, mismatch losses are evaluated by identifying the variance between the power achieved at the full irradiance and the power achieved at PSCs. They are determined as

$$\%\Delta P_{loss} = \frac{P_{stc} - P_{psc}}{P_{stc}} \times 100 \quad (22)$$

in which $\%\Delta P_{loss}$ is the percentage mismatch loss, P_{stc} is the power achieved at the full irradiance, and P_{psc} is the power achieved during PSCs.

The complexity in the MPPT control can be made lower by using only one variable for perturbation but the complexity increases if more than one perturbation variable is used to observe the power variation. The extended P&O MPPT algorithm in this paper utilizes voltage reference as a perturbing factor to observe the variation in power output.

The dual-input qZSI with two PV array inputs is compared with the implemented topology to highlight the additional PV input used in the implemented topology [21]. Similarly, a 2-MW grid-connected PV system in Navrongo, a town in Northern Ghana, is compared with the implemented topology to highlight the better use of the P&O algorithm with higher efficiency [20]. The performance of the proposed topology is observed to be equally good as both the dual-input qZSI and GUANYA inverter based on the qualitative comparative analysis in Table 4. The quantitative and qualitative comparison between other topologies proves that the grid-connected TI-3L-NPC-qZSI can efficiently harvest optimum energy from three PV inputs using a single MPPT controller.

8. Conclusions

A dynamic modeling and small signal analysis of the TI-3L-NPC-qZSI were performed. The small signal modeling of this topology is used to ensure system stability. The usage of three PV inputs does not increase the number of passive and active elements, being cost-effective. In addition, the size of the passive elements is not larger than in standard qZSI topologies, making the converter more compact. The relationship between the voltages and the currents of three PV inputs is derived from the small signal modeling, which shows that the voltages of PV_2 and PV_3 must always be equal, and the power of PV_1 must be greater

than the other two, and thus the current generated from PV_1 is higher. The primary focus of the work was to understand the feasibility and application of a low-voltage rooftop PV system utilizing TI-3L-NPC-qZSI topology. It is not easy to achieve the MPP when using three panels. Therefore, an extended MPPT algorithm based on the perturb and observe concept is used to address this issue. This idea is cost-effective as it uses only one MPPT controller. Based on simulation results, it can be confirmed that the control arrangement and design topology can perform well in power mismatch scenarios. The low voltage generated from the PV system is boosted and power with good quality is supplied to the grid. In a nutshell, the use of a single MPPT controller for three PV panels for a rooftop PV system is proposed in this article.

Author Contributions: Conceptualization, B.G. and Y.Y.; methodology, B.G.; software, B.G.; validation, B.G., Y.Y., A.M.A. and R.; formal analysis, B.G.; investigation, B.G.; resources, Y.Y.; data curation, B.G.; writing—original draft preparation, B.G.; writing—review and editing, B.G., Y.Y., A.M.A. and R.; visualization, B.G.; supervision, Y.Y. All authors have read and agreed to the published version of the manuscript.

Funding: This research received no external funding.

Data Availability Statement: The article contains all the data used.

Acknowledgments: The author would like to thank the Power Electronics Control and Integration Laboratory (PENCIL) for providing the funds and resources for research work.

Conflicts of Interest: The authors declare no conflicts of interest.

Abbreviations

Photovoltaic	PV
Maximum power point tracking	MPPT
Perturb and observe	P&O
Quasi-Z-source inverter	qZSI
Shoot-through	ST
Maximum power point	MPP
Partial shading conditions	PSCs
Partial shading	PS
Power-Voltage	P-V
Current-Voltage	I-V
Global maximum power point	GMPP
Three-level neutral-point-clamped quasi-Z-source inverter	3L-NPC-qZSI
Triple-input 3L-NPC-qZSI	TI-3L-NPC-qZSI
Quasi-Z-source	qZS
Pulse width modulation	PWM
Full-ST	FST
Non-ST	NST
Upper-ST	UST
Lower-ST	LST
Standard test conditions	STCs
Neutral-point-clamped	NPC
Fill-factor	FF

References

1. Forouzesh, M.; Siwakoti, Y.P.; Gorji, S.A.; Blaabjerg, F.; Lehman, B. Step-Up DC–DC Converters: A Comprehensive Review of Voltage-Boosting Techniques, Topologies, and Applications. *IEEE Trans. Power Electron.* **2017**, *32*, 9143–9178. [CrossRef]
2. Ding, T.; Li, C.; Yang, Y.; Jiang, J.; Bie, Z.; Blaabjerg, F. A Two-Stage Robust Optimization for Centralized-Optimal Dispatch of Photovoltaic Inverters in Active Distribution Networks. *IEEE Trans. Sustain. Energy* **2017**, *8*, 744–754. [CrossRef]
3. Morrison, A.; Zapata, J.W.; Kouro, S.; Perez, M.A.; Meynard, T.A.; Renaudineau, H. Partial power DC-DC converter for photovoltaic two-stage string inverters. In Proceedings of the 2016 IEEE Energy Conversion Congress and Exposition (ECCE), Milwaukee, WI, USA, 18–22 September 2016; pp. 1–6. [CrossRef]

4. Peng, F.Z. Z-source inverter. *IEEE Trans. Ind. Appl.* **2003**, *39*, 504–510. [CrossRef]
5. Li, Y.; Anderson, J.; Peng, F.Z.; Liu, D. Quasi-Z-Source Inverter for Photovoltaic Power Generation Systems. In Proceedings of the 2009 Twenty-Fourth Annual IEEE Applied Power Electronics Conference and Exposition, Washington, DC, USA, 15–19 February 2009; pp. 918–924. [CrossRef]
6. Elmorshedy, M.F.; Essawy, I.J.A.; Rashad, E.M.; Islam, M.R.; Dabour, S.M. A Grid-Connected PV System Based on Quasi-Z-Source Inverter with Maximum Power Extraction. *IEEE Trans. Ind. Appl.* **2023**, *59*, 6445–6456. [CrossRef]
7. Zhou, Y.; Wu, Q.; Li, Z.; Hong, F. Research on a Time-Variant Shoot-Through Modulation Strategy for Quasi-Z-Source Inverter. *IEEE Trans. Power Electron.* **2018**, *33*, 9104–9109. [CrossRef]
8. Le, H.-P.N.; Pham, K.D.; Nguyen, N. Analyses, Modeling, and SVPWM Control of a Three-Level T-NPC Inverter to Reduce Common-Mode Voltage Under Open-Circuit Fault in a Neutral-Point Switch. *IEEE Access* **2024**, *12*, 104708–104727. [CrossRef]
9. Zeb, K.; Uddin, W.; Khan, M.A.; Ali, Z.; Ali, M.U.; Christofides, N.; Kim, H.J. A comprehensive review on inverter topologies and control strategies for grid connected photovoltaic system. *Renew. Sustain. Energy Rev.* **2018**, *94*, 1120–1141. [CrossRef]
10. Celanovic, N.; Boroyevich, D. A comprehensive study of neutral-point voltage balancing problem in three-level neutral-point-clamped voltage source PWM inverters. *IEEE Trans. Power Electron.* **2000**, *15*, 242–249. [CrossRef]
11. Esram, T.; Chapman, P.L. Comparison of Photovoltaic Array Maximum Power Point Tracking Techniques. *IEEE Trans. Energy Convers.* **2007**, *22*, 439–449. [CrossRef]
12. Alhusseini, H.; Niroomand, M.; Mirzaeian Dehkordi, B. A Fuzzy-Based Adaptive P&O MPPT Algorithm for PV Systems with Fast Tracking and Low Oscillations Under Rapidly Irradiance Change Conditions. *IEEE Access* **2024**, *12*, 84374–84386. [CrossRef]
13. Nkambule, M.S.; Nabil Hasan, A.; Shongwe, T. Advanced Control Strategies for Photovoltaic Power Quality and Maximum Power Point Tracking Optimization. *IEEE Access* **2024**, *12*, 74456–74481. [CrossRef]
14. Kumar, M.; Panda, K.P.; Rosas-Caro, J.C.; Valderrabano-Gonzalez, A.; Panda, G. Comprehensive Review of Conventional and Emerging Maximum Power Point Tracking Algorithms for Uniformly and Partially Shaded Solar Photovoltaic Systems. *IEEE Access* **2023**, *11*, 31778–31812. [CrossRef]
15. Singh, S.; Sonar, S. Improved Maximum Boost Control and Reduced Common-Mode Voltage Switching Patterns of Three-Level Z-Source Inverter. *IEEE Trans. Power Electron.* **2021**, *36*, 6557–6571. [CrossRef]
16. Sahoo, M.; Keerthipati, S. A Three-Level LC-Switching-Based Voltage Boost NPC Inverter. *IEEE Trans. Ind. Electron.* **2017**, *64*, 2876–2883. [CrossRef]
17. Gupta, K.K.; Ranjan, A.; Bhatnagar, P.; Sahu, L.K.; Jain, S. Multilevel Inverter Topologies with Reduced Device Count: A Review. *IEEE Trans. Power Electron.* **2016**, *31*, 135–151. [CrossRef]
18. Schweizer, M.; Kolar, J.W. Design and Implementation of a Highly Efficient Three-Level T-Type Converter for Low-Voltage Applications. *IEEE Trans. Power Electron.* **2013**, *28*, 899–907. [CrossRef]
19. Li, Y.; Jiang, S.; Cintron-Rivera, J.G.; Peng, F.Z. Modeling and Control of Quasi-Z-Source Inverter for Distributed Generation Applications. *IEEE Trans. Ind. Electron.* **2013**, *60*, 1532–1541. [CrossRef]
20. Anto, E.K.; Asumadu, J.A.; Okyere, P.Y. PID control for improving P&O-MPPT performance of a grid-connected solar PV system with Ziegler-Nichols tuning method. In Proceedings of the 2016 IEEE 11th Conference on Industrial Electronics and Applications (ICIEA), Hefei, China, 5–7 June 2016; pp. 1847–1852. [CrossRef]
21. Lashab, A.; Sera, D.; Martins, J.; Guerrero, J.M. Dual-Input Quasi-Z-Source PV Inverter: Dynamic Modeling, Design, and Control. *IEEE Trans. Ind. Electron.* **2020**, *67*, 6483–6493. [CrossRef]
22. Gyawali, B.; Ajmal, A.M.; Liu, W.; Yang, Y. A Review on Modulation Techniques of Quasi-Z-Source Inverter for Grid-Connected Photovoltaic Systems. *E-Prime—Adv. Electr. Eng. Electron. Energy* **2024**, *10*, 100809. [CrossRef]
23. Ge, B.; Abu-Rub, H.; Peng, F.Z.; Lei, Q.; de Almeida, A.T.; Ferreira, F.J.T.E.; Sun, D.; Liu, Y. An Energy-Stored Quasi-Z-Source Inverter for Application to Photovoltaic Power System. *IEEE Trans. Ind. Electron.* **2013**, *60*, 4468–4481. [CrossRef]
24. Rukhsar; Ajmal, A.M.; Gyawali, B.; Yang, Y. Enhancing Power Generation in Photovoltaic Systems: A Comparison of AI Techniques. In Proceedings of the 2024 IEEE Workshop on Control and Modeling for Power Electronics (COMPEL), Lahore, Pakistan, 24–27 June 2024; pp. 1–7. [CrossRef]
25. Ali, A.; Almutairi, K.; Padmanaban, S.; Tirth, V.; Algarni, S.; Irshad, K.; Islam, S.; Zahir, M.H.; Shafiullah, M.; Malik, M.Z. Investigation of MPPT Techniques Under Uniform and Non-Uniform Solar Irradiation Condition–A Retrospection. *IEEE Access* **2020**, *8*, 127368–127392. [CrossRef]
26. Dadkhah, J.; Niroomand, M. Optimization Methods of MPPT Parameters for PV Systems: Review, Classification, and Comparison. *J. Mod. Power Syst. Clean Energy* **2021**, *9*, 225–236. [CrossRef]
27. Debnath, D.; Chatterjee, K. Maximising power yield in a transformerless single-phase grid connected inverter servicing two separate photovoltaic panels. *IET Renew. Power Gener.* **2016**, *10*, 1087–1095. [CrossRef]
28. Singh, N.; Jain, S.K. Investigation of three-level NPC-qZS inverter-based grid-connected renewable energy system. *IET Power Electron.* **2020**, *13*, 1071–1085. [CrossRef]

Disclaimer/Publisher's Note: The statements, opinions and data contained in all publications are solely those of the individual author(s) and contributor(s) and not of MDPI and/or the editor(s). MDPI and/or the editor(s) disclaim responsibility for any injury to people or property resulting from any ideas, methods, instructions or products referred to in the content.